

First Observation of $\tau \rightarrow 3\pi\eta\nu_\tau$ and $\tau \rightarrow f_1\pi\nu_\tau$ Decays

T. Bergfeld,¹ B. I. Eisenstein,¹ J. Ernst,¹ G. E. Gladding,¹ G. D. Gollin,¹ R. M. Hans,¹ E. Johnson,¹ I. Karliner,¹ M. A. Marsh,¹ M. Palmer,¹ M. Selen,¹ J. J. Thaler,¹ K. W. Edwards,² A. Bellerive,³ R. Janicek,³ D. B. MacFarlane,³ P. M. Patel,³ A. J. Sadoff,⁴ R. Ammar,⁵ P. Baringer,⁵ A. Bean,⁵ D. Besson,⁵ D. Coppage,⁵ C. Darling,⁵ R. Davis,⁵ N. Hancock,⁵ S. Kotov,⁵ I. Kravchenko,⁵ N. Kwak,⁵ S. Anderson,⁶ Y. Kubota,⁶ S. J. Lee,⁶ J. J. O'Neill,⁶ S. Patton,⁶ R. Poling,⁶ T. Riehle,⁶ V. Savinov,⁶ A. Smith,⁶ M. S. Alam,⁷ S. B. Athar,⁷ Z. Ling,⁷ A. H. Mahmood,⁷ H. Severini,⁷ S. Timm,⁷ F. Wappler,⁷ A. Anastassov,⁸ S. Blinov,^{8,*} J. E. Duboscq,⁸ D. Fujino,^{8,†} K. K. Gan,⁸ T. Hart,⁸ K. Honscheid,⁸ H. Kagan,⁸ R. Kass,⁸ J. Lee,⁸ M. B. Spencer,⁸ M. Sung,⁸ A. Undrus,^{8,*} R. Wanke,⁸ A. Wolf,⁸ M. M. Zoeller,⁸ B. Nemati,⁹ S. J. Richichi,⁹ W. R. Ross,⁹ P. Skubic,⁹ M. Bishai,¹⁰ J. Fast,¹⁰ E. Gerndt,¹⁰ J. W. Hinson,¹⁰ N. Menon,¹⁰ D. H. Miller,¹⁰ E. I. Shibata,¹⁰ I. P. J. Shipsey,¹⁰ M. Yurko,¹⁰ L. Gibbons,¹¹ S. Glenn,¹¹ S. D. Johnson,¹¹ Y. Kwon,¹¹ S. Roberts,¹¹ E. H. Thorndike,¹¹ C. P. Jessop,¹² K. Lingel,¹² H. Marsiske,¹² M. L. Perl,¹² D. Ugolini,¹² R. Wang,¹² X. Zhou,¹² T. E. Coan,¹³ V. Fadeyev,¹³ I. Korolkov,¹³ Y. Maravin,¹³ I. Narsky,¹³ V. Shelkov,¹³ J. Staeck,¹³ R. Stroynowski,¹³ I. Volobouev,¹³ J. Ye,¹³ M. Artuso,¹⁴ A. Efimov,¹⁴ M. Gao,¹⁴ M. Goldberg,¹⁴ D. He,¹⁴ S. Kopp,¹⁴ G. C. Moneti,¹⁴ R. Mountain,¹⁴ S. Schuh,¹⁴ T. Skwarnicki,¹⁴ S. Stone,¹⁴ G. Viehhauser,¹⁴ X. Xing,¹⁴ J. Bartelt,¹⁵ S. E. Csorna,¹⁵ V. Jain,¹⁵ K. W. McLean,¹⁵ S. Marka,¹⁵ R. Godang,¹⁶ K. Kinoshita,¹⁶ I. C. Lai,¹⁶ P. Pomianowski,¹⁶ S. Schrenk,¹⁶ G. Bonvicini,¹⁷ D. Cinabro,¹⁷ R. Greene,¹⁷ L. P. Perera,¹⁷ G. J. Zhou,¹⁷ B. Barish,¹⁸ M. Chadha,¹⁸ S. Chan,¹⁸ G. Eigen,¹⁸ J. S. Miller,¹⁸ C. O'Grady,¹⁸ M. Schmidler,¹⁸ J. Urheim,¹⁸ A. J. Weinstein,¹⁸ F. Würthwein,¹⁸ D. W. Bliss,¹⁹ G. Masek,¹⁹ H. P. Paar,¹⁹ S. Prell,¹⁹ V. Sharma,¹⁹ D. M. Asner,²⁰ J. Gronberg,²⁰ T. S. Hill,²⁰ R. Kutschke,²⁰ D. J. Lange,²⁰ S. Menary,²⁰ R. J. Morrison,²⁰ H. N. Nelson,²⁰ T. K. Nelson,²⁰ C. Qiao,²⁰ J. D. Richman,²⁰ D. Roberts,²⁰ A. Ryd,²⁰ M. S. Witherell,²⁰ R. Balest,²¹ B. H. Behrens,²¹ W. T. Ford,²¹ H. Park,²¹ J. Roy,²¹ J. G. Smith,²¹ J. P. Alexander,²² C. Bebek,²² B. E. Berger,²² K. Berkelman,²² K. Bloom,²² D. G. Cassel,²² H. A. Cho,²² D. M. Coffman,²² D. S. Crowcroft,²² M. Dickson,²² P. S. Drell,²² K. M. Ecklund,²² R. Ehrlich,²² A. D. Foland,²² P. Gaidarev,²² R. S. Galik,²² B. Gittelmann,²² S. W. Gray,²² D. L. Hartill,²² B. K. Heltsley,²² P. I. Hopman,²² J. Kandaswamy,²² P. C. Kim,²² D. L. Kreinick,²² T. Lee,²² Y. Liu,²² G. S. Ludwig,²² J. Masui,²² J. Mevissen,²² N. B. Mistry,²² C. R. Ng,²² E. Nordberg,²² M. Ogg,^{22,‡} J. R. Patterson,²² D. Peterson,²² D. Riley,²² A. Soffer,²² B. Valant-Spaight,²² C. Ward,²² M. Athanas,²³ P. Avery,²³ C. D. Jones,²³ M. Lohner,²³ C. Prescott,²³ J. Yelton,²³ J. Zheng,²³ G. Brandenburg,²⁴ R. A. Briere,²⁴ A. Ershov,²⁴ Y. S. Gao,²⁴ D. Y.-J. Kim,²⁴ R. Wilson,²⁴ H. Yamamoto,²⁴ T. E. Browder,²⁵ F. Li,²⁵ Y. Li,²⁵ and J. L. Rodriguez²⁵

(CLEO Collaboration)

¹University of Illinois, Champaign-Urbana, Illinois 61801

²Carleton University, Ottawa, Ontario, Canada K1S 5B6,
and the Institute of Particle Physics, Montréal, Québec, Canada

³McGill University, Montréal, Québec, Canada H3A 2T8,
and the Institute of Particle Physics, Montréal, Québec, Canada

⁵Ithaca College, Ithaca, New York 14850

⁵University of Kansas, Lawrence, Kansas 66045

⁶University of Minnesota, Minneapolis, Minnesota 55455

⁷State University of New York at Albany, Albany, New York 12222

⁸The Ohio State University, Columbus, Ohio 43210

⁹University of Oklahoma, Norman, Oklahoma 73019

¹⁰Purdue University, West Lafayette, Indiana 47907

¹¹University of Rochester, Rochester, New York 14627

¹²Stanford Linear Accelerator Center, Stanford University, Stanford, California 94309

¹³Southern Methodist University, Dallas, Texas 75275

¹⁴Syracuse University, Syracuse, New York 13244

¹⁵Vanderbilt University, Nashville, Tennessee 37235

¹⁶Virginia Polytechnic Institute and State University, Blacksburg, Virginia 24061

¹⁷Wayne State University, Detroit, Michigan 48202

¹⁸California Institute of Technology, Pasadena, California 91125

¹⁹University of California, San Diego, La Jolla, California 92093

²⁰University of California, Santa Barbara, California 93106

²¹University of Colorado, Boulder, Colorado 80309-0390

²²Cornell University, Ithaca, New York 14853

²³University of Florida, Gainesville, Florida 32611²⁴Harvard University, Cambridge, Massachusetts 02138²⁵University of Hawaii at Manoa, Honolulu, Hawaii 96822

(Received 25 June 1997)

We have observed new channels for τ decays with an η in the final state. We study 3-prong tau decays, using the $\eta \rightarrow \gamma\gamma$ and $\eta \rightarrow 3\pi^0$ decay modes and 1-prong decays with two π^0 's using the $\eta \rightarrow \gamma\gamma$ channel. The measured branching fractions are $\mathcal{B}(\tau^- \rightarrow \pi^- \pi^- \pi^+ \eta \nu_\tau) = (3.4_{-0.5}^{+0.6} \pm 0.6) \times 10^{-4}$ and $\mathcal{B}(\tau^- \rightarrow \pi^- 2\pi^0 \eta \nu_\tau) = (1.4 \pm 0.6 \pm 0.3) \times 10^{-4}$. We observe clear evidence for $f_1 \rightarrow \eta \pi \pi$ substructure and measure $\mathcal{B}(\tau^- \rightarrow f_1 \pi^- \nu_\tau) = (5.8_{-1.3}^{+1.4} \pm 1.8) \times 10^{-4}$. We have also searched for $\eta'(958)$ production and obtain 90% C.L. upper limits $\mathcal{B}(\tau^- \rightarrow \pi^- \eta' \nu_\tau) < 7.4 \times 10^{-5}$ and $\mathcal{B}(\tau^- \rightarrow \pi^- \pi^0 \eta' \nu_\tau) < 8.0 \times 10^{-5}$. [S0031-9007(97)04088-X]

PACS numbers: 13.35.Dx

Tau decays with an η meson in the final state provide important information about various hadronic symmetries and allow for a study of the resonant structure of the weak hadronic current [1,2]. These decays are rare and their detection became possible only recently with the high statistics CLEO experiment at Cornell Electron Storage Ring (CESR). Two such decays with small branching fractions already have been observed: $\mathcal{B}(\tau^- \rightarrow \pi^- \pi^0 \eta \nu_\tau) = (0.17 \pm 0.02 \pm 0.02)\%$ [3] and $\mathcal{B}(\tau^- \rightarrow K^- \eta \nu_\tau) = (0.026 \pm 0.005 \pm 0.005)\%$ [4,5]. Both channels also have been seen by the ALEPH group [6]. All other tau decays involving η mesons were expected to be severely suppressed. The decay $\tau \rightarrow 3\pi \eta \nu_\tau$ can proceed through the axial-vector current and its branching fraction was predicted to be 1.2×10^{-6} [1].

In this Letter, we present the first observation of the tau decay $\tau \rightarrow 3\pi \eta \nu_\tau$ using three final states: $\pi^- \pi^+ \pi^- \eta \gamma \gamma$, where η is reconstructed from the $\eta \rightarrow \gamma\gamma$ decay; $\pi^- \pi^+ \pi^- \eta 3\pi^0$, where η is reconstructed from its $\eta \rightarrow 3\pi^0$ decay; and $\pi^- 2\pi^0 \eta \gamma \gamma$, where η is reconstructed from the $\eta \rightarrow \gamma\gamma$ decay and the remaining photons from $2\pi^0$'s. In addition, for the first time, we observe $\tau^- \rightarrow f_1 \pi^- \nu_\tau$ using the $f_1 \rightarrow \eta \pi^+ \pi^-$ decay mode. We also search for decays with $\eta'(958)$ using the $\eta' \rightarrow \eta \pi^+ \pi^-$ decay mode with $\eta \rightarrow \gamma\gamma$.

We use data obtained by the CLEO II detector [7] at the CESR operating at a center of mass energy corresponding to the peak of the $Y(4S)$ resonance ($E_{c.m.} = 10.6$ GeV) and 60 MeV below this energy. The data correspond to an integrated luminosity of 4.68 fb^{-1} and contain about 4.27 million $\tau^+ \tau^-$ pairs. CLEO II is a general purpose solenoidal spectrometer. In addition to good quality tracking, its special feature is a 7800 crystal CsI(Tl) electromagnetic calorimeter that provides photon detection with high efficiency and good energy and angular resolution, which is essential for η and π^0 reconstruction.

We select events using the 1 vs 3 and 1 vs 1 charged track topologies and tag one of the tau decays with a single charged track in the drift chamber which is required to be identified as an electron, muon, or hadron. The electron candidate is required to have momentum, p , greater than 0.5 GeV and energy deposition in the calorimeter, E , such that $0.9 < E/p < 1.1$. If specific ionization (dE/dx) information is available, we veto the

event if it is more than 2 standard deviations below the expected value. Muon candidates must penetrate at least three adsorption lengths of material for track momenta less than 2.0 GeV, and more than five adsorption lengths for momenta above 2.0 GeV.

A hadron tag is a track not identified as an electron or muon and with momentum pointing to the barrel part of the calorimeter, $|\cos \theta| < 0.81$, where θ is the polar angle defined with respect to the beam direction. The invariant mass, including all photon candidates in the tag hemisphere, is required to be less than 1.2 GeV. In addition to single pions, this tag recovers unidentified electrons and muons and a large fraction of $\tau^- \rightarrow \rho^- \nu_\tau$ decays.

The second tau—representing the signal candidate—is reconstructed from its decays into $\pi^- \pi^+ \pi^- \eta \gamma \gamma$, $\pi^- \pi^+ \pi^- \eta 3\pi^0$, and $\pi^- 2\pi^0 \eta \gamma \gamma$ final states. We assume that all charged tracks are pions since there is very little phase space for decays in which one of the tracks is a kaon. The dE/dx information is consistent with this assumption.

Photons are identified by isolated energy clusters in the calorimeter, separated from energy deposits left by charged tracks and with photonlike lateral profiles of energy deposition. Photon candidates used for π^0 and η reconstruction are required to be in the barrel part of the calorimeter and to satisfy $|S_{\gamma\gamma}^X| < 10$, where $S_{\gamma\gamma}^X \equiv (m_{\gamma\gamma} - m_X)/\sigma_{\gamma\gamma}$ ($X = \pi^0$ or η) and $\sigma_{\gamma\gamma}$ is the π^0 or η mass resolution (~ 12 MeV). Only photon pair combinations with $-3.0 < S_{\gamma\gamma}^{\pi^0} < 2.0$ are considered as signal candidates; those with larger values of $|S_{\gamma\gamma}^{\pi^0}|$ are used for sidebands.

For lepton (hadron) tags, the lower energy photon used for η reconstruction must have energy greater than 200 (250) MeV and the higher energy photon must have energy greater than 400 (700) MeV. Photons used to form π^0 's are required to have energies greater than 30 MeV. In events for which more than one combination of photons passes all cuts, we choose the combination with the smallest χ^2 for that signal hypothesis.

We suppress $e^+ e^- \rightarrow e^+ e^- (\gamma)$ and $e^+ e^- \rightarrow \mu^+ \times \mu^- (\gamma)$ events by vetoing events with tracks which have energy greater than 85% of the beam energy. To remove background due to two-photon processes, we require the

missing momentum vector of the event to be in the angular region $|\cos \theta| < 0.9$. We suppress contributions from tau decays with a K_S in the final state by requiring that for all tracks, the impact parameter with respect to the interaction point must be less than 5 mm. Background from low multiplicity $q\bar{q}$ events and incompletely reconstructed tau events is minimized by rejecting events with additional isolated photons with an energy greater than 120 MeV. To further reduce $q\bar{q}$ background, we require the total invariant mass of the hadrons in the signal hemisphere to be less than the tau mass.

For the $\pi^-\pi^+\pi^-\eta_{\gamma\gamma}$ sample we reduce $q\bar{q}$ and two-photon backgrounds by requiring the event to have missing mass satisfying $0.1 < M_{\text{miss}}/E_{\text{c.m.}} < 0.5$ and total transverse momentum greater than 0.3 GeV [8]. Decays with K_S 's are additionally suppressed by requiring both $\pi^+\pi^-$ combinations to have a mass at least 15 MeV from the K_S mass. To suppress background from events with gamma conversions, we veto events with electron candidates in the signal hemisphere.

We simulate tau signal and background events using the KORALB generator and TAUOLA decay packages [9] (with some modifications discussed below) and measured tau branching fractions [10]; GEANT [11] is used for detector simulation.

We find background associated with various QED processes to be negligible by using Monte Carlo (MC) simulations and independent data samples. To estimate $q\bar{q}$ background, we use independent data samples requiring the invariant mass of the tag hemisphere to be greater than 1.8 GeV. We select predominantly hadronic events satisfying the same topological and kinematic requirements on the signal hemisphere as described above, except for the tau mass cut. The normalization for this hadronic sample is obtained from a fit to the data in the region with signal invariant mass above 1.8 GeV.

The distributions illustrating η signal in all three analyses are shown in Fig. 1. Tau background contributes almost entirely through random $\gamma\gamma$ combinations while most of the coherent η background comes from $q\bar{q}$ events. Distributions of hadronic masses for events from the η signal regions are shown in Fig. 2, where the events with masses above the tau mass are plotted as well. Signal regions for $\eta \rightarrow \gamma\gamma$ and $\eta \rightarrow 3\pi^0$ channels are $-3.0 < S_{\gamma\gamma}^{\eta} < 2.0$ and $|M(3\pi^0) - M_{\eta}| < 20$ MeV, respectively.

We extract the number of η 's by fitting the distributions shown in Fig. 1. In Table I we present results from the three analyses. Efficiencies shown in Tables I and II include tagging branching fractions.

We estimate several sources of systematic errors. The major contributions are (for $\pi^-\pi^+\pi^-\eta_{\gamma\gamma}$, $\pi^-\pi^+ \times \pi^-\eta_{3\pi^0}$, and $\pi^-\pi^+\pi^-\eta_{\gamma\gamma}$ samples) π^0 and η reconstruction efficiency (10%, 10%, 4%); model dependence (5%, 23%, 10%); backgrounds (15%, 17%, 18%). The total systematic errors are 19%, 33%, and 20%, respectively. One of the major sources of systematic errors is the uncertainty in the modeling of showers generated by the in-

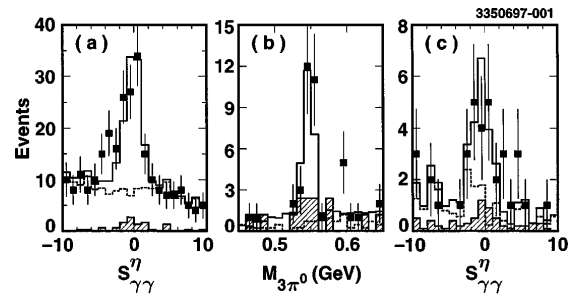


FIG. 1. Distribution of η mass for the (a) $\pi^-\pi^+\pi^-\eta_{\gamma\gamma}$, (b) $\pi^-\pi^+\pi^-\eta_{3\pi^0}$, and (c) $\pi^-\pi^+\pi^-\eta_{\gamma\gamma}$ samples. The solid line is a fit to the data (squares). The tau and $q\bar{q}$ backgrounds are indicated by the dashed line and hatched area, respectively. Plots (a) and (c) are binned in units of $S_{\gamma\gamma}^{\eta}$ while (b) has a 10 MeV bin size. In (b), the energies and angles of each photon of the π^0 candidates have been constrained to π^0 mass.

teractions of charged particles in the calorimeter and this uncertainty increases for higher charged multiplicity final states. Other contributions to the systematic errors include the uncertainty in the detector acceptance, track finding efficiency, luminosity measurement, and $\tau^+\tau^-$ production cross section.

For the $\pi^-\pi^+\pi^-\eta_{\gamma\gamma}$ sample, there is enough data for a consistency check of $\mathcal{B}(\tau \rightarrow \pi^-\pi^+\pi^-\eta\nu_{\tau})$ measurements among data samples selected with e , μ , and hadron tags. They are consistent with each other, with a χ^2 of 5.1 for three degrees of freedom, corresponding to a 16% confidence level. Combining $\pi^-\pi^+\pi^-\eta_{\gamma\gamma}$ and $\pi^-\pi^+\pi^-\eta_{3\pi^0}$ results, we obtain $\mathcal{B}(\tau \rightarrow \pi^-\pi^+\pi^-\eta\nu_{\tau}) = (3.4^{+0.6}_{-0.5} \pm 0.6) \times 10^{-4}$.

A $3\pi\eta$ final state could proceed through a number of different resonances. In Fig. 3 for events from the η signal region we plot the $\pi\eta$ vs $\eta\pi\pi$ mass distributions, using the mass-constrained η and π^0 momenta. The distributions show higher population density in the $f_1(1285)/a_0(980)$ region, indicating the presence of the decay chain: $\tau^- \rightarrow f_1\pi^-\nu_{\tau}$, $f_1 \rightarrow a_0(980)\pi$, $a_0(980) \rightarrow \eta\pi$. For the 3-prong modes [Figs. 3(a) and 3(b)] there is an ambiguity in the choice of the same charge pions that results in four entries per event. In the case of $\tau^- \rightarrow \pi^-2\pi^0\eta\nu_{\tau}$ [Fig. 3(c)], there is only one $f_1 \rightarrow \eta\pi^0\pi^0$

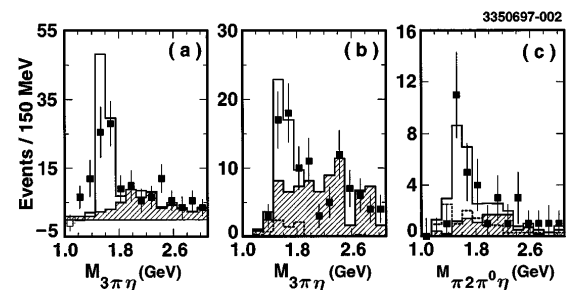


FIG. 2. Hadronic mass spectra for the (a) $\pi^-\pi^+\pi^-\eta_{\gamma\gamma}$ (after η sideband subtraction), (b) $\pi^-\pi^+\pi^-\eta_{3\pi^0}$, and (c) $\pi^-\pi^+\pi^-\eta_{\gamma\gamma}$ samples. The solid line is a fit to the data (squares). The tau and $q\bar{q}$ backgrounds are indicated by the dashed line and hatched area, respectively.

TABLE I. The number of data signal events, efficiencies, and branching fractions for the three data analyses. The signal has been corrected for the background.

Sample	N_{data}^{η}	ε [%]	$\mathcal{B} (\times 10^{-4})$
$\pi^{-}\pi^{+}\pi^{-}\eta_{\gamma\gamma}$	$73.4_{-12.3}^{+13.0}$	6.3	$3.5_{-0.6}^{+0.7} \pm 0.7$
$\pi^{-}\pi^{+}\pi^{-}\eta_{3\pi^0}$	$15.2_{-4.6}^{+4.8}$	1.8	$3.1_{-0.9}^{+0.9} \pm 1.0$
$\pi^{-}2\pi^0\eta_{\gamma\gamma}$	$15.0_{-5.0}^{+5.0}$	2.5	$1.4_{-0.6}^{+0.6} \pm 0.3$

combination and two $\eta\pi^0$ combinations. Since the kinematics of the $f_1 \rightarrow a_0\pi^0$ decay are such that the higher mass $\eta\pi^0$ combination is the correct one about 90% of the time, we plot only the higher-mass $\eta\pi^0$ combination.

We expect that more than 75% of all $f_1 \rightarrow \eta\pi\pi$ decays proceed through the $a_0(980)\pi$ state [10]. To extract the number of the $f_1\pi$ events we perform a binned maximum likelihood fit. We restrict the fit to the area shown in Fig. 3 to avoid the kinematically forbidden region and we weight each event by the inverse of the number of entries. The fit function is the sum of a signal MC a_0 vs f_1 distribution, a random $\gamma\gamma$ background shape obtained from nonsignal tau MC and a constant background. For the signal MC we use the full decay chain with f_1 and $a_0(980)$ resonances [12] and include all $\eta\pi\pi$ and $\eta\pi$ mass combinations. The constant background accounts for a possible non- f_1 signal. To take into account the uncertainty in the random $\gamma\gamma$ background normalization, we perform a combined fit of the $M(\pi\eta)$ vs $M(\pi\pi\eta)$ and $S_{\gamma\gamma}$ data distributions with normalizations of the random $\gamma\gamma$ background constrained to be the same. From Monte Carlo studies we find that all three fits have confidence levels above 18%. We have found no sources of background which can contribute to the f_1 peak.

In Table II we show the fit results obtained for the different data samples. We have used $\mathcal{B}(f_1(1285) \rightarrow \eta\pi\pi) = 0.54 \pm 0.15$ [10] and an isospin factor of 2/3 (1/3) for $\eta\pi^+\pi^-(\eta\pi^0\pi^0)$. We include a systematic error of 28% to account for the uncertainty of the $f_1 \rightarrow \eta\pi\pi$ decay rate. All other contributions to the total systematic error including different models of the $f_1 \rightarrow \eta\pi\pi$ decay are found to be much smaller. The total systematic error is 33% for all three channels.

The weighted average for all three channels is $\mathcal{B}(\tau^- \rightarrow f_1\pi^-\nu_\tau) = (5.8_{-1.3}^{+1.4} \pm 1.8) \times 10^{-4}$. Using results from the $\pi^{-}\pi^{+}\pi^{-}\eta_{\gamma\gamma}$ channel we find the ratio $\mathcal{B}(\tau^- \rightarrow f_1\pi^-\nu_\tau \rightarrow \pi^{-}\pi^{+}\pi^{-}\eta_{\nu_\tau})/\mathcal{B}(\tau^- \rightarrow \pi^{-}\pi^{+}\pi^{-}\eta_{\nu_\tau}) = 0.55 \pm 0.14$. Here we take advantage of the fact that

TABLE II. The number of signal events, efficiencies, and branching fractions for the $\tau^- \rightarrow f_1\pi^-\nu_\tau$ decays obtained from fits.

Sample	$N_{\text{data}}^{f_1}$	ε [%]	$\mathcal{B} (\times 10^{-4})$
$\pi^{-}\pi^{+}\pi^{-}\eta_{\gamma\gamma}$	$36.3_{-9.0}^{+9.7}$	5.6	$5.3_{-1.3}^{+1.4} \pm 1.8$
$\pi^{-}\pi^{+}\pi^{-}\eta_{3\pi^0}$	$9.6_{-4.7}^{+5.6}$	1.4	$6.8_{-3.3}^{+4.0} \pm 2.2$
$\pi^{-}2\pi^0\eta_{\gamma\gamma}$	$8.4_{-3.2}^{+3.2}$	2.6	$6.6_{-2.5}^{+2.5} \pm 2.3$

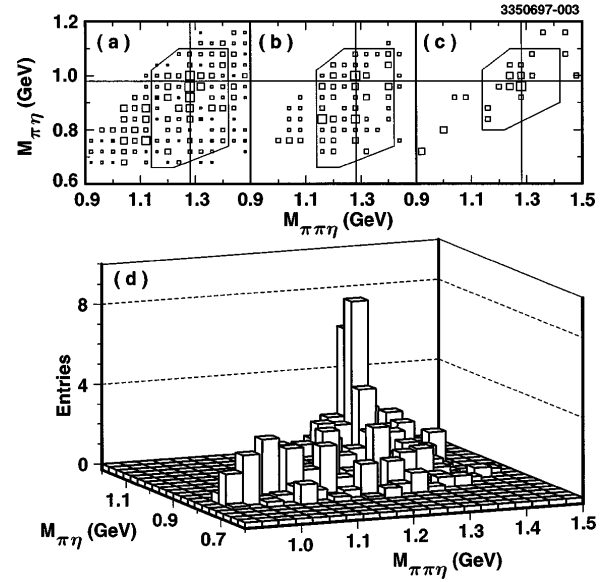


FIG. 3. $M(\pi\eta)$ vs $M(\pi\pi\eta)$ for the (a) $\pi^{-}\pi^{+}\pi^{-}\eta_{\gamma\gamma}$ (after η sideband subtraction), (b) $\pi^{-}\pi^{+}\pi^{-}\eta_{3\pi^0}$, and (c) $\pi^{-}2\pi^0\eta_{\gamma\gamma}$ samples. Plot (d) is a sum of (a), (b), and (c) weighted as 0.25, 0.25, and 1, respectively. All bin widths are 40 MeV.

some systematic uncertainties are canceled in the ratio. It would appear that not all of the $\pi^{-}\pi^{+}\pi^{-}\eta$ final state proceeds through an intermediate f_1 . This accounts for the difference between the Monte Carlo shape and the data in Fig. 2(a). We show in Fig. 4 the background-subtracted distribution of $M(\pi^{-}\pi^{+}\pi^{-}\eta)$ calculated for $\pi^{-}\pi^{+}\pi^{-}\eta_{\gamma\gamma}$ events with a $\pi^{+}\pi^{-}\eta$ mass of at least 36 MeV from the nominal f_1 mass. This distribution as well as distributions of all other submass projections is consistent with $\tau^- \rightarrow a_1(1260)^-\eta\nu_\tau \rightarrow \pi^-\rho^0\eta\nu_\tau$ decay model. Since the observed excess has less than 2.0σ significance, we set an upper limit: $\mathcal{B}(\tau^- \rightarrow a_1(1260)^-\eta\nu_\tau \rightarrow \pi^-\rho^0\eta\nu_\tau) < 3.9 \times 10^{-4}$ at 90% C.L.

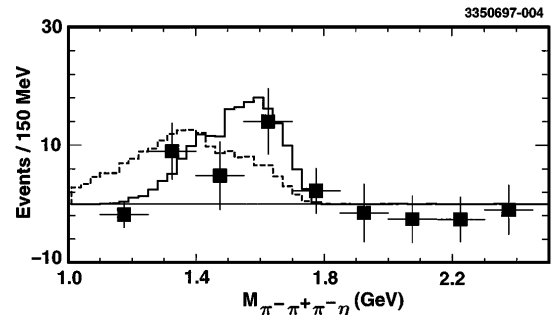


FIG. 4. Distribution of $\pi^{-}\pi^{+}\pi^{-}\eta$ invariant mass plotted for $\pi^{-}\pi^{+}\pi^{-}\eta_{\gamma\gamma}$ events not associated with $\tau^- \rightarrow f_1\pi^-\nu_\tau$ decay. The Monte Carlo expectations for the decays $\tau^- \rightarrow \rho^0\pi^-\eta\nu_\tau$ and $\tau^- \rightarrow a_1(1260)^-\eta\nu_\tau \rightarrow \pi^{-}\pi^{+}\pi^{-}\eta\nu_\tau$ are shown as dashed and solid lines, respectively. Both Monte Carlo modes are generated via phase space with ‘‘V-A’’ factor [12].

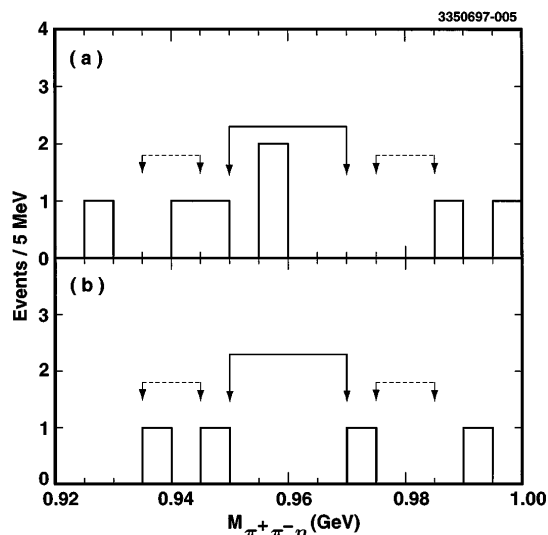


FIG. 5. Distribution of the $M_{\pi^+\pi^-\eta}$ plotted for (a) $\tau^- \rightarrow \pi^-\eta'(958)\nu_\tau$ and (b) $\tau^- \rightarrow \pi^-\pi^0\eta'(958)\nu_\tau$ signal candidates. The solid (dashed) arrows indicate the signal (sideband) regions.

The measured branching fraction for the decay $\tau^- \rightarrow \pi^-\pi^+\pi^-\eta\nu_\tau$ is more than 2 orders of magnitude larger than the value calculated by Pich [1] under the assumption that this decay is dominated by an ηa_1 intermediate state. In a recent calculation, Li [13] used similar assumptions to obtain $\mathcal{B}(\tau^- \rightarrow a_1(1260)^-\eta\nu_\tau \rightarrow \pi^-\rho^0\eta\nu_\tau) = 2.93 \times 10^{-4}$. In another paper, Li [14] calculated $\mathcal{B}(\tau^- \rightarrow f_1\pi^-\nu_\tau) = 2.9 \times 10^{-4}$, which is still somewhat smaller than the present measurement.

The decay $\tau \rightarrow 3\pi\eta\nu_\tau$ has important implications for the phenomenology of the multipion τ decays, especially for $\tau \rightarrow 6\pi\nu_\tau$. Several authors [15–17] have used isospin relations [18] to calculate the relative amounts of $\tau^- \rightarrow 3\pi^-2\pi^+\pi^0\nu_\tau$, $\tau^- \rightarrow \pi^-\pi^+\pi^-3\pi^0\nu_\tau$ and $\tau^- \rightarrow \pi^-5\pi^0\nu_\tau$, and claimed some discrepancies between the measured branching fractions and conserved vector current (CVC) predictions obtained from the $e^+e^- \rightarrow 6\pi$ measurements.

It now appears that $\tau^- \rightarrow 3\pi^-2\pi^+\pi^0\nu_\tau$ and $\tau^- \rightarrow \pi^-\pi^+\pi^-3\pi^0\nu_\tau$ decays have large contributions from the $\tau \rightarrow 3\pi\eta\nu_\tau$ channel. Since this final state has opposite G parity to that of the direct 6π decays and proceeds through an axial-vector current, its contribution must be subtracted before applying isospin relations or using CVC to compare with e^+e^- annihilation data.

We use the selected samples of $\tau^- \rightarrow \pi^-\pi^+\pi^-\eta\nu_\tau$ events to set upper limits on the $\tau^- \rightarrow \pi^-\eta'(958)\nu_\tau$ and $\tau^- \rightarrow \pi^-\pi^0\eta'(958)\nu_\tau$ decays. Each event must contain an η candidate: $0.51 \text{ GeV} < M_\eta < 0.57 \text{ GeV}$. For the second decay, the remaining photons with $E_\gamma > 30 \text{ MeV}$ are used for the π^0 reconstruction. In the $M_{\pi^+\pi^-\eta}$ signal (sideband) region shown in Figs. 5(a) and 5(b) we find 2 (1) and 0 (1) events, respectively. The event detection efficiencies are 4.4% and 2.3%, with relative systematic uncertainties of 11% and 15.6%, respectively. Using

Poisson statistics and assuming a linear background distribution we obtain [19] $\mathcal{B}(\tau^- \rightarrow \pi^-\eta'(958)\nu_\tau) < 7.4 \times 10^{-5}$ and $\mathcal{B}(\tau^- \rightarrow \pi^-\pi^0\eta'(958)\nu_\tau) < 8.0 \times 10^{-5}$.

We gratefully acknowledge the effort of the CESR staff in providing us with excellent luminosity and running conditions. This work was supported by the National Science Foundation, the U.S. Department of Energy, the Heisenberg Foundation, the Alexander von Humboldt Stiftung, Research Corporation, the Natural Sciences and Engineering Research Council of Canada, and the A. P. Sloan Foundation.

*Permanent address: BINP, RU-630090 Novosibirsk, Russia.

†Permanent address: Lawrence Livermore National Laboratory, Livermore, CA 94551.

‡Permanent address: University of Texas, Austin, TX 78712.

- [1] A. Pich, Phys. Lett. B **196**, 561 (1987).
- [2] H. Neufeld and H. Rupertsberger, Z. Phys. C **68**, 91 (1995).
- [3] CLEO Collaboration, M. Artuso *et al.*, Phys. Rev. Lett. **69**, 3278 (1992).
- [4] CLEO Collaboration, J. Bartelt *et al.*, Phys. Rev. Lett. **76**, 4119 (1996).
- [5] Throughout this paper charge conjugation is implied.
- [6] ALEPH Collaboration, D. Buskulic *et al.*, Z. Phys. C **74**, 263 (1997).
- [7] CLEO Collaboration, Y. Kubota *et al.*, Nucl. Instrum. Methods Phys. Res., Sect. A **320**, 66 (1992).
- [8] $M_{\text{miss}} = \sqrt{(E_{\text{c.m.}} - E_{\text{vis}})^2 - P_{\text{vis}}^2}$, where E_{vis} and P_{vis} are the total visible energy and momentum of the event, respectively.
- [9] KORALB (v.2.1), S. Jadach and Z. Was, Comput. Phys. Commun. **36**, 191 (1985); **64**, 267 (1991); **85**, 453 (1995); TAUOLA (v.1.5), S. Jadach, J.H. Kühn, and Z. Was, Comput. Phys. Commun. **64**, 275 (1991); **70**, 69 (1992); **76**, 361 (1993).
- [10] Particle Data Group, R. M. Barnett *et al.*, Phys. Rev. D **54**, 1 (1996).
- [11] GEANT 3.15, R. Brun *et al.*, Report No. CERN DD/EE/84-1.
- [12] Monte Carlo events are generated according to phase space with a $V-A$ factor, $(M_\tau^2 - q^2)^2(M_\tau^2 + 2q^2)$, and a P-wave barrier factor $8p_\pi^3/q^3$, where p_π is the momentum of the pion in the $f_1\pi$ center of mass and q is the total effective mass of the hadrons. We assume the decay spectral function to be dominated by the form factor of the $a_1(1260)$ resonance.
- [13] B. A. Li, hep-ph/9702316.
- [14] B. A. Li, Phys. Rev. D **55**, 1436 (1997).
- [15] A. Donnachie and A. B. Clegg, Phys. Rev. D **51**, 4979 (1995).
- [16] R. Sobie, Z. Phys. C **69**, 99 (1995).
- [17] A. Rouge, Z. Phys. C **70**, 65 (1996).
- [18] A. Pais, Ann. Phys. (Paris) **9**, 548 (1960).
- [19] K. K. Gan, J. Lee, and R. Kass, Report No. OHSTPY-HEP-E-97-009.